Stability of a Shock-Decelerated Ablation Front

Y. Aglitskiy,[1] M. Karasik,[2] A. L. Velikovich,[2] V. Serlin,[2] J. L. Weaver,[2] A. J. Schmitt,[2] S. P. Obenschain,[2] N. Metzler,[3] S. T. Zalesak,[4] J. H. Gardner,[4] J. Oh,[5] and E. C. Harding[6]

[1]*Science Applications International Corporation, McLean, Virginia 22150, USA*
[2]*Plasma Physics Division, Naval Research Laboratory, Washington, D.C. 20375, USA*
[3]*Artep Inc., Colombia, Maryland 20145, USA*
and Department of Mechanical Engineering, Ben Gurion University, Beer Sheva, Israel
[4]*Berkeley Research Associates, Beltsville, Maryland 20705, USA*
[5]*Research Support Instruments, Lanham, Maryland 20706, USA*
[6]*University of Michigan, Ann Arbor, Michigan 48109, USA*

(Received 23 March 2009; published 17 August 2009)

Experimental study of a shock-decelerated ablation front is reported. A planar solid plastic target is accelerated by a laser across a vacuum gap and collides with a lower-density plastic foam layer. While the target is accelerated, a fast Rayleigh-Taylor (RT) growth of the seeded single-mode perturbation at the ablation front is observed. After the collision, the velocity of the ablation front is seen to remain constant. The reshock quenches the RT growth but does not trigger any Richtmyer-Meshkov growth at the ablation front, which is shown to be consistent with both theory and simulations.

DOI: 10.1103/PhysRevLett.103.085002 PACS numbers: 52.57.Fg, 47.20.Ma, 52.35.Tc, 52.70.La

Instability of the ablation front in the imploded laser target remains one of the key issues of laser fusion. Ignition and high gain are only possible if the Rayleigh-Taylor (RT) growth of the perturbations seeded in the vicinity of the ablation front remains within reasonable limits throughout the acceleration and deceleration phases of the implosion. The exponentially growing RT eigenmodes are developed from the target and irradiation nonuniformities through the physical process called RT seeding. Seeding proceeds during the early phase of the implosion when the target is being compressed, before it starts to accelerate. A major role in the RT seeding is played by the interaction of the shock and rarefaction waves in the target with the ablation front via a variety of mechanisms such as ablative Richtmyer-Meshkov (RM) instability [1–7] and feedout [4,7–12].

Interaction of multiple shock waves with ablation fronts plays a particularly important role in the new approaches to direct-drive laser fusion, such as shock ignition [13] and multiple-picket target adiabat shaping [14]. Shock ignition [13] requires a fast recompression of an expanding central hot spot with a converging shock wave driven by a short, powerful ''ignitor'' laser pulse irradiating the target at peak compression. The strong ignitor shock wave reshocks the inner shell surface (the boundary of the hot spot), which itself represents an ablation front [15]. The multiple-picket approach [14] replaces a constant-intensity ''foot'' or a gradual rise of the laser pulse with several short pulses, which drive shocks into the target through the ablation front.

Our experiments on the Nike laser at the Naval Research Laboratory (NRL) are aimed at obtaining observational data and thereby at improving our understanding of the dynamics of shocked ablation fronts, propagation and interactions of shock and rarefaction waves, and perturbation development in accelerated, coasting, and decelerated targets. The experiments presented here were made possible by improving the imaging capability of our x-ray diagnostics.

A shocked material interface exhibits the classical RM instability [16]. An ablation front responds to a shock wave in a different way. Theory, simulations, and experiments [1–7] are all in agreement that a shocked ablation front is stable. When ramped laser intensity drives a shock wave through the ablation front into the dense target, the ablation front experiences small-amplitude, low-frequency decaying oscillations. The mechanisms that make the ablation front stable with respect to the RM-type growth [17], unlike a material interface, are (1) the ''rocket effect'' [18] or ''dynamic overpressure'' [2], which provides the restoring force causing the oscillations, and (2) the mass flow through the ablation front, which is responsible for their damping (see the detailed discussion in [2,4,6]).

All the simulations and experiments reported so far [1–7] refer to the ''light-to-heavy'' case, when the shock wave originates at the ablation front and propagates from it into the dense target plasma. According to the theory [2,6], stability of a nonaccelerated ablation front is an intrinsic property. Therefore the theory predicts that the ablation front should remain stable even when the shock wave arrives from the dense target plasma (the ''heavy-to-light'' case). This prediction has never been tested before. We report the results of experiments and simulations designed to test the theory for this case.

Figure 1 illustrates our target design and the diagnostics. The targets consist of a 25–30 μm thick planar plastic (CH) foil rippled on the rear side (single-mode ripple wavelength $\lambda = 45$ μm, peak-to-valley amplitude 2 μm)

 © 2009 The American Physical Society

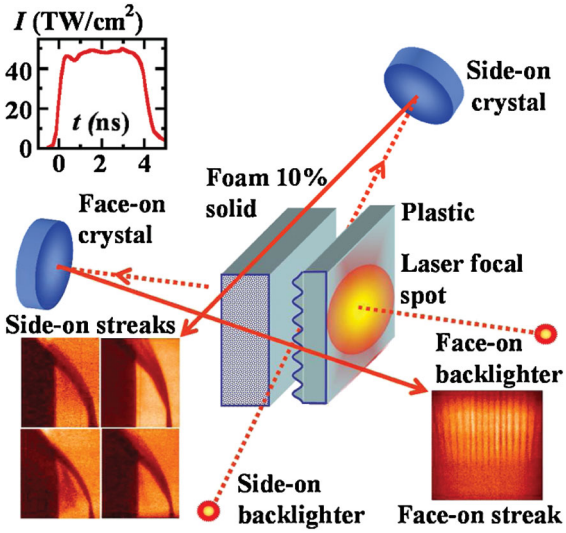

FIG. 1 (color). Orthogonal x-ray imaging diagnostics implemented on the Nike laser.

and a ~200 μm thick planar layer of divinyl benzene foam (10%–20% of solid CH density) separated from the CH foil by a 100–120 μm wide vacuum gap. The front side of the plastic foil is irradiated by 37 overlapping beams of the Nike krypton fluoride laser ($\lambda_L = 248$ nm) [19]. The Nike laser produces a very uniform irradiation with a time-averaged rms nonuniformity <0.3% in a central region of the focal spot, which is 400 μm in diameter. The Nike pulse used in our experiments has a nearly rectangular temporal shape with a 4 ns FWHM, 0.4 ns rise time (see the inset in Fig. 1).

We have improved our diagnostics to enable a detailed simultaneous study of the one-dimensional (1D) dynamics of shock and ablation fronts (side-on imaging) and the two-dimensional (2D) areal mass perturbation development in laser-driven targets (face-on imaging). The Nike orthogonal monochromatic x-ray imaging system is based on Bragg reflection from spherically curved crystals [3,4,7,20]. The energy of 12 Nike beams, ~500 J, is delivered to one or two silicon backlighter targets producing x rays that backlight and/or sidelight the main target for about 5 ns. A spherically curved quartz crystal selects the resonance line of the He-like Si (1.86 keV) and projects a monochromatic image of the target on the slit of the x-ray streak camera. Face-on and side-on images are formed by two separate backlighters and spherically bent crystals. The face-on streak record (Fig. 1, right) shows the 2D evolution of areal mass perturbations in the target [3,4,7,12,21]. The monochromatic x-ray imaging makes it possible to translate the observed modulation of the optical thickness directly into the modulation of the areal mass. The side-on streak records (left) show the 1D time history of the CH foil acceleration, plastic-on-foam collision, the propagation of shock waves, and the dynamics of the ablation front. Obtaining unambiguous side-on images of extended targets is not easy since the line of sight parallel to the target surface inevitably includes areas illuminated by laser flux densities ranging from zero to the maximum. Alignment of a double-foil target with the gap of 75–100 μm also presents a challenge. We substantially mitigated both problems by using narrow targets with the width close to the central part of the focal distribution (~500 μm); see Fig. 1.

Figure 2 demonstrates the simulated and observed 1D time history of a collision for a target with a 30 μm thick CH foil separated by a 120 μm gap from a 200 μm thick, 10% solid CH density foam layer. Figure 2(a) is a simulated density map on the (x, t) plane. The laser irradiation drives a strong shock wave into the CH foil, compresses it and sets it into the motion at constant mass velocity that is associated with the shock wave. Before the start of its acceleration, the trajectory of the ablation front on the (x, t) plane is straight. The compressed CH foil plasma starts to accelerate following the breakout of this shock at its rear surface, when the rarefaction wave reflected from it reaches the ablation front ($t \approx 1.4$ ns). The acceleration makes the trajectory of the ablation front on the (x, t) plane convex. Then at $t \approx 3$ ns the foil accelerated to ~10^7 cm/s collides with the foam layer. Simulations indicate that the collision briefly produces a pressure of ~30 Mbar, which is 3.5 times greater than the pressure ~8 Mbar maintained by the laser at the ablation front. This pressure pulse generates two strong shock waves. One of them propagates forward into the thick foam layer, while the other propagates back into the thin, compressed, and partly ablated CH foil plasma. The ablation front is re-

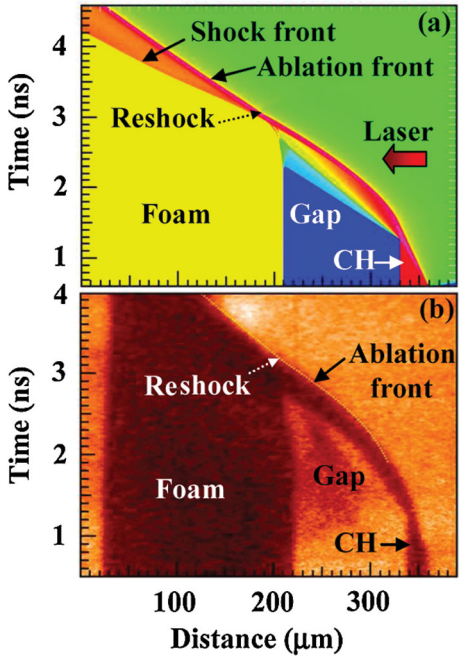

FIG. 2 (color). Simulated density map (a) and side-on x-ray streak record (b) for a CH foil collision with a foam layer.

shocked from the dense plasma side. The ablation front rapidly decompresses from the high shock pressure to ~8 Mbar. The rarefaction wave that emerges from the ablation front at the instant of its reshock carries the reduced pressure back to the shock wave propagating into the foam, rapidly slowing it down. This shock is then fully determined by the ablative pressure maintained by the laser ablation and the foam density, as evidenced by the shape of this shock's (x, t) trajectory on Fig. 2(a), which is concave for a short time interval, and then a straight line after $t \approx 3.2$ ns. The reshock impulsively changes the velocity of the ablation front, which then stays constant, and its (x, t) trajectory becomes straight again starting from $t \approx 3.1$ ns.

The 1D dynamics of the foil acceleration and collision is visible in the side-on streak record shown in Fig. 2(b) in greater detail than ever before. We observe the shock compression of the CH foil and its subsequent evolution into a constant-mass-velocity motion [straight (x, t) trajectory], which is followed by its acceleration [parabolic (x, t) trajectory] and then by its collision with the foam layer. After the collision, the observed (x, t) trajectory of the ablation front becomes straight again, confirming that its acceleration indeed ends at collision.

Figure 3 compares velocities of the shocks in 10% solid density foam produced by direct irradiation of the foam with Nike beams (a) and by collision of the laser-accelerated CH foil with the foam layer (b). The slope of the dashed lines exactly corresponds to the shock velocity in the latter case, averaged from the instant of collision to the observed shock breakout at the rear surface, and it is very close to the observed velocity of the shock wave driven into the foam directly by the laser. The constant velocities of the shock front in the foam and of the ablation fronts at this stage are fully determined by the ablative pressure maintained by the laser and the foam density.

Observed and simulated evolution of the dominant Fourier mode of the areal mass modulation is shown in Fig. 4. The thick lines with approximate error bars present the experimental data from the face-on images. The pink line corresponds to the same conditions as Fig. 2, the light blue line to a higher foam density: 10% and 20% of solid, respectively. The signal is normalized with respect to its initial value corresponding to the peak-to-valley 2 μm ripple amplitude of solid plastic. The small time shift between these two curves prior to the collision is due to a combination of difference in the actual foil thickness and the timing relative to the start of the laser pulse. The thin red line and the thin blue line show the simulation results obtained in two-dimensional simulations for the same conditions as the pink line and the light blue line, respectively, using the FAST2D hydrocode developed at NRL [22] with plasma radiation taken into account.

After the start of the laser pulse, the simulated time histories show that each of the areal mass modulation amplitudes δm passes through a minimum, changes its phase twice, and then starts to grow. This is a signature of the lateral mass redistribution in the rippled rarefaction wave emerged from the rippled rear surface of the CH foil after the shock breakout, as explained in [11] and observed in our experiments [4,12] (for details, see the Appendix

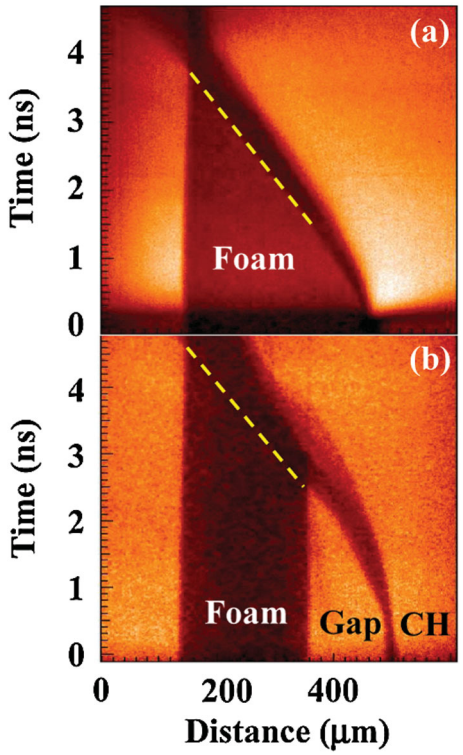

FIG. 3 (color). Side-on x-ray streak records for a directly irradiated 10% solid density foam layer (a) and a CH foil colliding with such a layer (b).

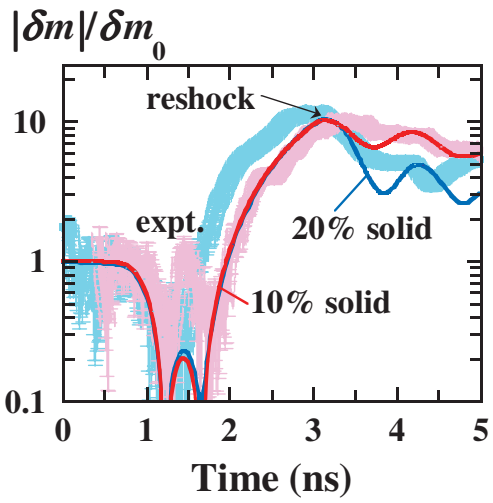

FIG. 4 (color). Observed (thick, with approximate error bars) and simulated (thin lines) time history of the areal mass modulation amplitude in the target. Arrow indicates the instant of reshock on simulated lines.

found in [23]). Figure 4 shows that the early-time minimum and two phase reversals are not well resolved in this experiment because our CH foil is thinner than those used in [4,12], and δm near the minimum is very small. Our observations are nevertheless consistent with the presence of this minimum and with the corresponding delay in the onset of the RT growth.

The RT growth is quenched when the collision occurs and the ablation front is reshocked. A reshock of a material interface would (re)start a classical RM growth of its perturbations. Since the linear RM growth rate is proportional to the initial ripple amplitude [16], a ''heavy-to-light'' reshock of a material interface after a substantial RT or RM amplification of its nonuniformities would give rise to a rapid growth of the areal mass modulation amplitude in the negative direction, implying a quick reversal of its phase [24]. A similar increase of the RM growth rate at a reshocked interface has been observed in shock-tube experiments [25]. Our results presented in Fig. 4 do not demonstrate such a behavior. Instead, the growth of the areal mass modulation amplitude is seen to end with the reshock and to be followed by decaying oscillations around a nonzero average value. This effect is robust and caused entirely by the collision. As demonstrated in the Appendix found in [23], the quenching is not due to nonlinear saturation or any other mechanism that would slow down the RT growth in the absence of the collision.

Decaying oscillations of a nonaccelerated ablation front have been predicted [1,2] and observed [3–5] during the early-time shock compression stage. It must be emphasized that the oscillations seen in Fig. 4 are of a different nature. First, their frequency is much higher than that of the slow oscillations of the ablation front driven by the ''rocket effect'' [18], which for our experimental conditions is $<0.1\ \mathrm{ns}^{-1}$ [4]. Second, these are oscillations around a nonzero average; hence, the ablation front ripples, which provide the largest contribution to the observed areal mass modulation amplitude δm, do not change phase. On the other hand, the simulated and observed oscillation period, ~ 1 ns, is close to the sound wave period λ/c_s, where $\lambda = 45\ \mu$m, and the speed of sound c_s in the reshocked foil plasma is estimated from the simulations to be $\sim 5 \times 10^6$ cm/s. The observed time history of δm therefore involves fast areal mass oscillations in the rippled rarefaction wave [4,11,12] that emerges from the ablation front after the reshock, superimposed upon the slow, also oscillatory, evolution due to the ablative RM instability [1–7]. Indeed, all our simulation results show that the changes in δm after the collision accumulate in the volume of the plasma rather than near the ablation front [23].

To summarize, we report the first observations of perturbation evolution in an ablation front, which is shocked from the dense plasma side. The plasma flow produced this way has much in common with the previously studied cases of ablative RM instability (triggered when a shock wave is launched from the ablation front to the target plasma [1–7]) and feedout (started when a shock wave breaks out at the free rear surface of the target [4,8–12]). Like the latter case, the process we observe starts when a shock wave breaks out and generates a rarefaction wave. Like the former case, the shocked surface is an ablation front. Our observations prove that the ablation front becomes stable as soon as its acceleration stops. Dynamics of the ablation front are directly observed, including the period of its motion following the collision of the laser-accelerated foil with a low-density foam layer, when its velocity stays constant after the reshock. We observe the RT growth of the perturbations prior to the reshock and the quenching of the growth thereafter. Thus we have demonstrated that the stability properties of an ablation front after its acceleration ends are the same as before its acceleration starts, in agreement with the theory [2,6].

The authors acknowledge the excellent technical support of Nike Laser Crew. This work was supported by the U.S. Department of Energy, Defense Programs.

[1] A. L. Velikovich *et al.*, Phys. Plasmas **5**, 1491 (1998).
[2] V. N. Goncharov, Phys. Rev. Lett. **82**, 2091 (1999).
[3] Y. Aglitskiy *et al.*, Phys. Rev. Lett. **87**, 265001 (2001).
[4] Y. Aglitskiy *et al.*, Phys. Plasmas **9**, 2264 (2002).
[5] O. V. Gotchev *et al.*, Phys. Rev. Lett. **96**, 115005 (2006).
[6] V. N. Goncharov *et al.*, Phys. Plasmas **13**, 012702 (2006).
[7] Y. Aglitskiy *et al.*, Phys. Scr. **T132**, 014021 (2008).
[8] R. Betti *et al.*, Phys. Rev. Lett. **81**, 5560 (1998).
[9] D. P. Smitherman *et al.*, Phys. Plasmas **6**, 932 (1999).
[10] K. Shigemori *et al.*, Phys. Rev. Lett. **84**, 5331 (2000).
[11] A. L. Velikovich *et al.*, Phys. Plasmas **8**, 592 (2001).
[12] Y. Aglitskiy *et al.*, Phys. Rev. Lett. **87**, 265002 (2001).
[13] R. Betti *et al.*, Phys. Rev. Lett. **98**, 155001 (2007); W. Theobald *et al.*, Phys. Plasmas **15**, 056306 (2008).
[14] V. N. Goncharov *et al.*, Bull. Am. Phys. Soc. **53**, 248 (2008); J. P. Knauer *et al.* Bull. Am. Phys. Soc. **53**, 248 (2008).
[15] R. Betti *et al.*, Phys. Plasmas **8**, 5257 (2001); J. Sanz and R. Betti, Phys. Plasmas **12**, 042704 (2005).
[16] R. D. Richtmyer, Commun. Pure Appl. Math. **13**, 297 (1960); E. E. Meshkov, Fluid Dyn. **4**, 101 (1972).
[17] A. L. Velikovich *et al.*, Phys. Plasmas **7**, 1662 (2000).
[18] J. Sanz, Phys. Rev. Lett. **73**, 2700 (1994); A. R. Piriz, J. Sanz, and L. F. Ibañez, Phys. Plasmas **4**, 1117 (1997).
[19] S. P. Obenschain *et al.*, Phys. Plasmas **3**, 2098 (1996).
[20] Y. Aglitskiy *et al.*, Appl. Opt. **37**, 5253 (1998).
[21] Y. Aglitskiy *et al.*, Phys. Plasmas **13**, 080703 (2006).
[22] A. J. Schmitt *et al.*, Phys. Plasmas **11**, 2716 (2004); N. Metzler *et al.*, Phys. Plasmas **6**, 3283 (1999).
[23] See EPAPS Document No. E-PRLTAO-103-021935 for the retrieval of the PDF file in which the Appendix to this work can be found. For more information on EPAPS, see http://www.aip.org/pubservs/epaps.html.
[24] A. L. Velikovich *et al.*, Bull. Am. Phys. Soc. **53**, 56 (2008).
[25] E. Leinov *et al.*, Phys. Scr. **T132**, 014014 (2008).